

Snapback-free shorted anode LIGBT with controlled anode barrier and resistance

Shun Li(李顺), Jin-Sha Zhang(张金沙), Wei-Zhong Chen(陈伟中), Yao Huang(黄垚), Li-Jun He(贺利军), and Yi Huang(黄义)

Citation: Chin. Phys. B, 2021, 30 (**2**): 028501. DOI: 10.1088/1674-1056/abb7fc
Journal homepage: http://cpb.iphy.ac.cn; http://iopscience.iop.org/cpb

What follows is a list of articles you may be interested in

Influences of increasing gate stem height on DC and RF performances of InAlAs/InGaAs InP-based HEMTs

Zhi-Hang Tong(童志航), Peng Ding(丁芃), Yong-Bo Su(苏永波), Da-Hai Wang(王大海), and Zhi Jin(金智)
Chin. Phys. B, 2021, 30 (**1**): 018501. DOI: 10.1088/1674-1056/abb30d

Design of a novel high holding voltage LVTSCR with embedded clamping diode

Ling Zhu(朱玲), Hai-Lian Liang(梁海莲), Xiao-Feng Gu(顾晓峰), Jie Xu(许杰)
Chin. Phys. B, 2020, 29 (**6**): 068503. DOI: 10.1088/1674-1056/ab836e

A snapback-free TOL-RC-LIGBT with vertical P-collector and N-buffer design

Weizhong Chen(陈伟中), Yao Huang(黄垚), Lijun He(贺利军), Zhengsheng Han(韩郑生), Yi Huang(黄义)
Chin. Phys. B, 2018, 27 (**8**): 088501. DOI: 10.1088/1674-1056/27/8/088501

An improved GGNMOS triggered SCR for high holding voltage ESD protection applications

Zhang Shuai, Dong Shu-Rong, Wu Xiao-Jing, Zeng Jie, Zhong Lei, Wu Jian
Chin. Phys. B, 2015, 24 (**10**): 108502. DOI: 10.1088/1674-1056/24/10/108502

A snapback suppressed reverse-conducting IGBT with uniform temperature distribution

Chen Wei-Zhong, Li Ze-Hong, Zhang Bo, Ren Min, Zhang Jin-Ping, Liu Yong, Li Zhao-Ji
Chin. Phys. B, 2014, 23 (**1**): 018505. DOI: 10.1088/1674-1056/23/1/018505

Snapback-free shorted anode LIGBT with controlled anode barrier and resistance*

Shun Li(李顺)[1], Jin-Sha Zhang(张金沙)[1], Wei-Zhong Chen(陈伟中)[1,2,†], Yao Huang(黄垚)[1], Li-Jun He(贺利军)[1], and Yi Huang(黄义)[1]

[1] College of Electronics Engineering, Chongqing University of Posts and Telecommunications, Chongqing 400065, China
[2] Institute of Microelectronics, Chinese Academy of Sciences, Beijing 100029, China

(Received 22 July 2020; revised manuscript received 1 September 2020; accepted manuscript online 14 September 2020)

A novel shorted anode lateral-insulated gate bipolar transistor (SA LIGBT) with snapback-free characteristic is proposed and investigated. The device features a controlled barrier $V_{barrier}$ and resistance R_{SA} in anode, named CBR LIGBT. The electron barrier is formed by the P-float/N-buffer junction, while the anode resistance includes the polysilicon layer and N-float. At forward conduction stage, the $V_{barrier}$ and R_{SA} can be increased by adjusting the doping of the P-float and polysilicon layer, respectively, which can suppress the unipolar mode to eliminate the snapback. At turn-off stage, the low-resistance extraction path (N-buffer/P-float/polysilicon layer /N-float) can quickly extract the electrons in the N-drift, which can effectively accelerate the turn-off speed of the device. The simulation results show that at the same V_{on} of 1.3 V, the E_{off} of the CBR LIGBT is reduced by 85%, 73%, and 59.6% compared with the SSA LIGBT, conventional LIGBT, and TSA LIGBT, respectively. Additionally, at the same E_{off} of 1.5 mJ/cm^2, the CBR LIGBT achieves the lowest V_{on} of 1.1 V compared with the other LIGBTs.

Keywords: shorted anode lateral-insulated gate bipolar transistor, snapback, barrier, trade-off

PACS: 85.30.De, 85.30.Pq, 85.30.Tv **DOI:** 10.1088/1674-1056/abb7fc

1. Introduction

Lateral insulated gate bipolar transistor (LIGBT) is a popular power device due to its voltage control and low power loss at forward conduction, which is widely used in the field of the power integrated circuits.[1–9] However, the excessive carriers in the N-drift lead to the large turn-off loss E_{off}.[10–17] The shorted anode (SA) LIGBT can effectively accelerate the extraction of electrons by introducing the N+ anode in anode.[18] However, the snapback effect is induced when the working mode of the device transforms from unipolar mode to bipolar mode. In order to solve this problem, several novel structures have been proposed. The separated shorted anode (SSA) LIGBT is adopted to suppress the snapback by controlling the distance between N+ anode and P+ anode.[19] The trench shorted anode (TSA) LIGBT is proposed to alleviate the snapback by inducing an oxide trench between N+ anode and P+ anode, which extends the path of the electrons.[20] The segmented trench in the anode region (STA) LIGBT can avoid the snapback by inducing a deep trench in anode.[21,22] The multiple current plugs (MCP) LIGBT can eliminate the snapback by introducing three separated current plugs into N-buffer.[23]

In this work, a novel SA LIGBT featuring a controlled anode barrier and resistance (CBR) is proposed and discussed to achieve the snapback-free and better trade-off characteristic between V_{on} and E_{off}. The devices simulation results and validations are obtained by the TCAD MEDICI tools, and the parallel field mobility model, concentration-dependent model, perpendicular electric field mobility model, auger recombination, and Shockley–Read–Hall recombination model are adopted.[24]

2. Device structure and mechanism

Figure 1(a) shows the schematic views of the CBR LIGBT. An oxide trench is set to be in anode region, which divides the N-drift into two parts. The P-float is set to be on the left of the oxide trench, which forms an electron barrier $V_{barrier}$ to inhibit the electrons from flowing into the N+ anode. The N-type doping polysilicon layer is located on the top of the oxide trench, while the N-float is set to be on the right of the oxide trench, which forms the anode resistance R_{SA} in series. The key parameters for the different structures compared with each other in this paper are listed in Table 1, where t and N_{poly} are the thickness and doping concentration of the polysilicon layer, respectively; N_{P-} and N_{N-} are the doping concentrations of the P-float and N-float, respectively; L_B is the distance between N+ anode and P+ anode of the SSA LIGBT; L_t is the length of oxide trench of the TSA LIGBT.

Figure 1(b) shows the equivalent circuit and operating mechanism of the CBR LIGBT. The polysilicon layer and N-float are respectively regarded as the R_1 and R_2 in series, while

*Project supported by the National Natural Science Foundation of China (Grant Nos. 61604027 and 61704016) and the Fund from Chongqing Technology Innovation and Application Development (Key Industry Research and Development), China (Grant No. cstc2018jszx-cyzd0646).

†Corresponding author. E-mail: cwz@cqu.edu.cn

© 2021 Chinese Physical Society and IOP Publishing Ltd

the P-float is an electron barrier to block electrons flowing into the N+ anode. The height of the potential barrier V_{barrier} is expressed as

$$V_{\text{barrier}} = \frac{k_0 T}{q}\left(\ln\frac{N_{\text{buffer}}\cdot N_{\text{P-}}}{n_{\text{i}}^2}\right), \tag{1}$$

where n_{i} is the intrinsic carrier concentration, N_{buffer} is the doping of the N-buffer, $N_{\text{P-}}$ and k_0 are the doping of the P-float and Boltzmann constant, respectively.

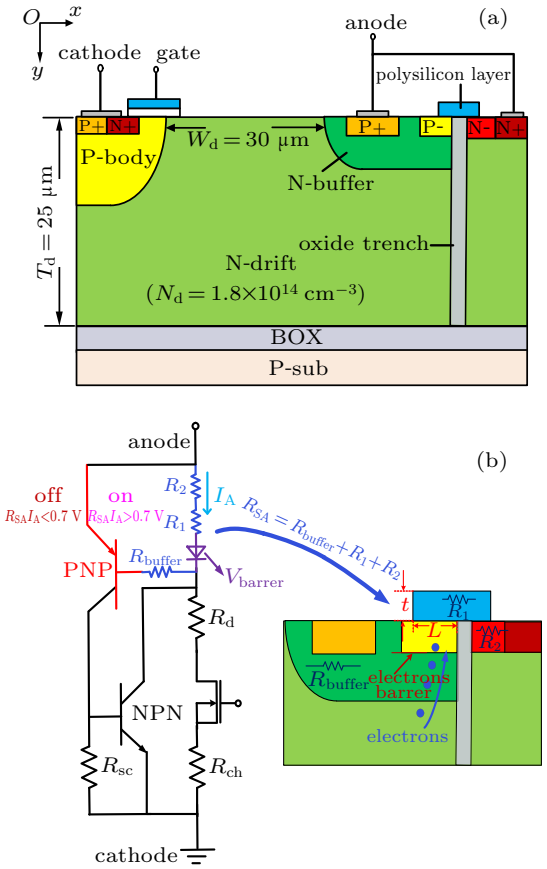


Fig. 1. (a) Schematic diagram of CBR LIGBT, N_{drift} doping $N_{\text{d}} = 1.8\times10^{14}$ cm^{-3}, N-drift length $W_{\text{d}} = 30$ μm. (b) Equivalent circuit and operating mechanism of CBR LIGBT in unipolar mode.

Table 1. Key parameters of different LIGBTs.

	CBR	SA	SSA	TSA
T_{d} (μm)	25	25	25	25
W_{d} (μm)	30	30	30	30
N_{d} (cm^{-3})	1.8×10^{14}	1.8×10^{14}	1.8×10^{14}	1.8×10^{14}
T_{Box} (μm)	2	2	2	2
T_{ox} (nm)	25	25	25	25
N_{buffer} (cm^{-3})	5×10^{15}	5×10^{15}	5×10^{15}	5×10^{15}
L_{B} (μm)	–	–	20	–
L_{t} (μm)	–	–	–	3
$N_{\text{P-}}$ (cm^{-3})	9×10^{15}	–	–	–
$N_{\text{N-}}$ (cm^{-3})	1×10^{16}	–	–	–
N_{poly} (cm^{-3})	1×10^{16}	–	–	–

The value of R_1 and R_2 can be obtained from

$$R_1 = \rho_{\text{poly}}\frac{L_{\text{poly}}}{S_{\text{poly}}} = \frac{L_{\text{poly}}}{N_{\text{poly}}q\mu t Z}, \tag{2}$$

$$R_2 = \rho_{\text{N-}}\frac{L_{\text{N-}}}{S_{\text{N-}}} = \frac{L_{\text{N-}}}{N_{\text{N-}}q\mu t_{\text{n}} Z}, \tag{3}$$

where L_{poly} and $L_{\text{N-}}$ are the length of the polysilicon layer and N-float, respectively, t_{n} is the thickness of the N-float, and Z is the length of the device in the vertical direction. Thus, the proposed device obtains a larger R_{SA} than the SA LIGBT. At the initial forward conduction stage ($I_{\text{A}}\cdot R_{\text{SA}} < 0.7$ V), the device operates in unipolar mode with single electrons, and the P-body/N-drift/P+ anode triode is turned off. When $I_{\text{A}}\cdot R_{\text{SA}} \geq 0.7$ V, the PNP transistor is turned on, and the P+ anode injects holes into the N-drift. The device works in the bipolar mode. When the device transforms from unipolar mode to bipolar mode, the turnover voltage of snapback effect V_{SB} can be approximated as the following expression:[25]

$$V_{\text{SB}} = V_{\text{PN}}\left(1+\frac{R_{\text{d}}+R_{\text{ch}}}{R_{\text{SA}}}\right) - V_{\text{barrier}}, \tag{4}$$

where R_{d} and R_{ch} are the resistance of N-drift region and channel, respectively; R_{SA} can be calculated from

$$R_{\text{SA}} = R_{\text{buffer}} + R_1 + R_2. \tag{5}$$

So, the snapback V_{SB} can be suppressed by increasing the V_{barrier}, R_1 or R_2 in the anode.

At turning off stage, the N-buffer/P-float/Polysilicon layer/N-float forms a low-resistance path to accelerate the extraction of electrons, which effectively reduces the E_{off} of the CBR LIGBT.

3. Results and discussion

3.1. Forward conduction characteristics

Figure 2(a) shows the comparison of forward conduction characteristics among the CBR LIGBT, SA LIGBT, SSA LIGBT, and TSA LIGBT. For the SA LIGBT, it switches from unipolar mode to bipolar mode with abrupt voltage due to the shorted effect of the N+ anode. Thus it exhibits the most serious snapback phenomenon in all the LIGBTs above. For the SSA LIGBT, it still suffers a tiny snapback even if the L_{B} increases to 20 μm, which leads to the waste of the chip length. For the TSA LIGBT, the snapback effect can be effectively suppressed when the oxide trench is deep enough ($L_{\text{t}} \geq 3$ μm). The CBR LIGBT achieves the snapback-free characteristic, because the R_{SA} and the V_{barrier} can be easily increased by adjusting the doping concentration of polysilicon layer and P-float. Additionally, both the CBR LIGBT and TSA LIGBT achieve the lowest voltage drop of 1.12 V at J_{A} of 100 A/cm^2.

Figure 2(b) shows the current distributions in the anode region of the CBR LIGBT at points A and B. At point A of $J_{\text{A}} = 3$ A/cm^2, the device operates in a unipolar mode, and the P+ anode/N-buffer junctions is turned off. The electron current flows to the N+ anode along the path of N-buffer/ P-float/ Polysilicon layer/ N-float. At point B of $J_{\text{A}} = 40$ A/cm^2,

the P+anode/N-buffer junction is turned on, and the P+ anode begins to inject holes into the N-drift. The device mode transforms into bipolar mode with exponentially increased current.

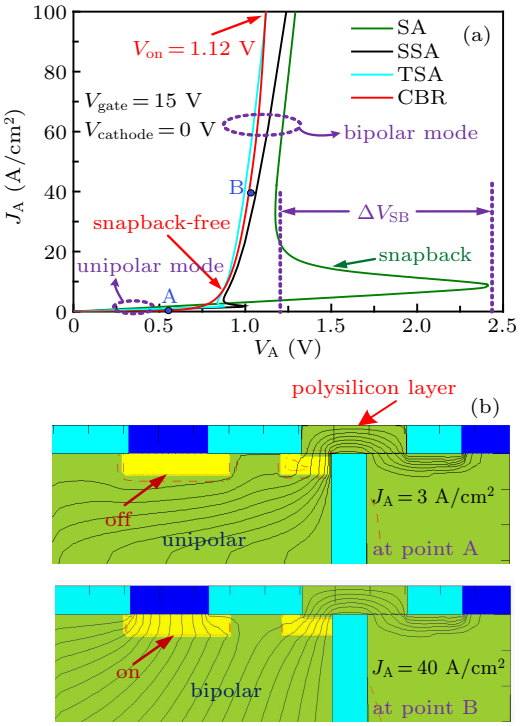


Fig. 2. (a) Forward conduction characteristics of CBR LIGBT, SA LIGBT, SSA LIGBT (L_B = 20 μm), and TSA LIGBT (L_t = 3 μm), with voltage applied to the gate V_{gate} being 15 V, and cathode connected to the ground $V_{cathode}$ = 0 V. (b) Current distributions in anode at points A and B of CBR LIGBT (points A and B are shown in (a)).

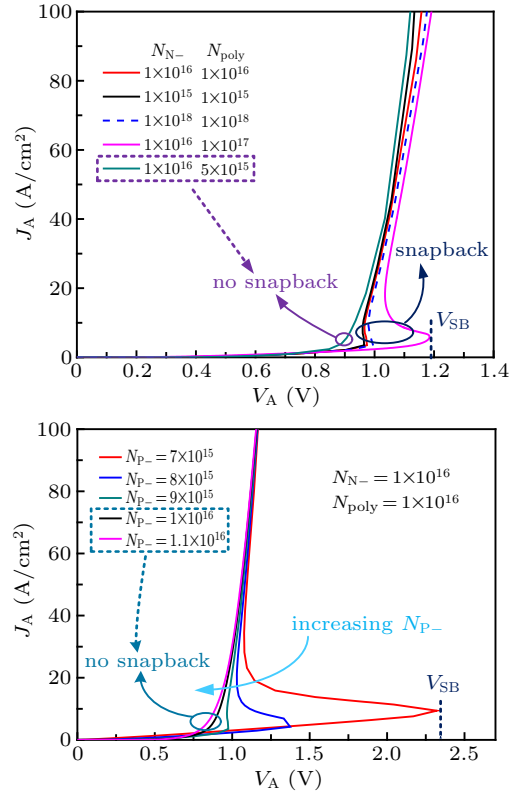


Fig. 3. Forward conduction characteristics of CBR LIGBT (a) at different values of N_{poly}, N_{N-}, and (b) N_{P-}.

Figure 3 shows the forward conduction characteristics of CBR LIGBT at different values of N_{P-}, N_{N-}, and N_{poly}. Obviously, the decreasing of N_{poly} and N_{N-} are favorable for suppressing the snapback because the R_1 and R_2 are increased as shown in Fig. 3(a). In Fig. 3(b), increasing N_{P-} is helpful in suppressing the snapback because the $V_{barrier}$ is increased according to Eqs. (1) and (4). Moreover, the inhibition effect of N_{P-} and N_{poly} on snapback are more obvious than that of N_{N-}. So adjusting N_{P-} and N_{poly} are a promising method to eliminate the snapback phenomenon.

Figure 4 shows the influences of N_{poly} on forward voltage drop V_{on} at different temperatures T of CBR LIGBT. For the given T, both the V_{on} and ΔV_{SB} gradually increase with N_{poly} increasing, and it also illustrates that reducing N_{poly} is beneficial to solving the snapback problem and reducing the V_{on}. In addition, at the same N_{poly}, V_{on} decreases obviously with the increase of T, and a higher temperature is also easier to achieve the snapback-free characteristic. This is because the mobility decreases with the increase of temperature, which leads to a larger R_{SA} for the CBR LIGBT. At T = 400 K, the device exhibits snapback effect only at N_{poly} of 1×10^{18} cm^{-3}.

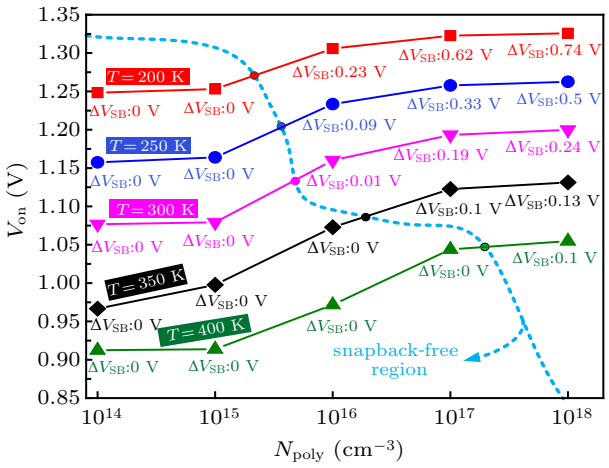


Fig. 4. Influences of N_{poly}on forward voltage drop V_{on} at different temperatures of CBR LIGBT, with V_{on} calculated at anode current density of 100 A/cm^2.

3.2. Turn off characteristics

In Fig. 5 the turn-off characteristics of different LIGBTs are compared among each other. All the devices are compared mutually at the same V_{on} of 1.3 V. The turnoff time T_{off} is calculated from 90% I_A to 10% I_A. For the SSA LIGBT, it shows the longest T_{off} of 570 ns, because a long L_B is designed to suppress the snapback and also reduce the V_{on}, resulting in a long extraction path with high resistance at turn-off stage. For the TSA LIGBT, it has T_{off} of 160 ns, because the trench oxide in anode will prevent the electrons from being extracted. The T_{off} of SA LIGBT is 90 ns, which is slightly slower than that of the CBR LIGBT. This is the result of a long and high doping concentration P+ anode necessary to achieve the V_{on} of 1.3 V, which is not conducive to the extraction of electrons.

For the CBR LIGBT, it achieves the shortest T_{off} of 70 ns, because the N-buffer/P-float/polysilicon layer/N-float provides a low-resistance path to accelerate the extraction of electrons in N-drift.

Figure 6 shows the distributions of the electron concentration N_e of different LIGBTs ($y = 4$ μm) from t_1 to t_4 period, and the devices start to be turned off at t_1 period. At t_2 and t_3 periods, the N_e of CBR LIGBT is lower obviously than that of the SSA LIGBT and TSA LIGBT. At t_4 period, the SA LIGBT and CBR LIGBT have completed the turn-off process, while there remain a lot of electrons in SSA LIGBT and TSA LIGBT.

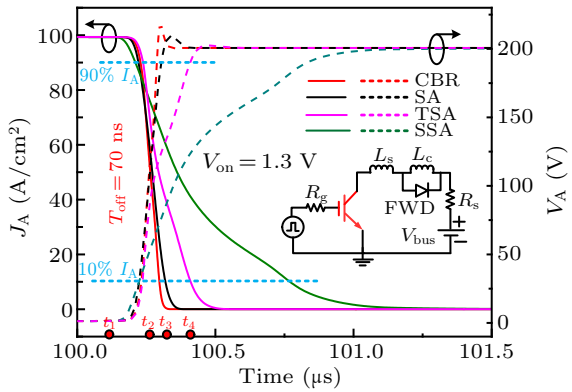


Fig. 5. Turn-off characteristics of different LIGBTs at the same V_{on} of 1.3 V, obtained in the same circuit with bus voltage (V_{bus}) 200 V, gate resistance (R_g) 10 Ω, load inductance (L_C) 10 μH, and stray inductance (L_s) 10 nH.

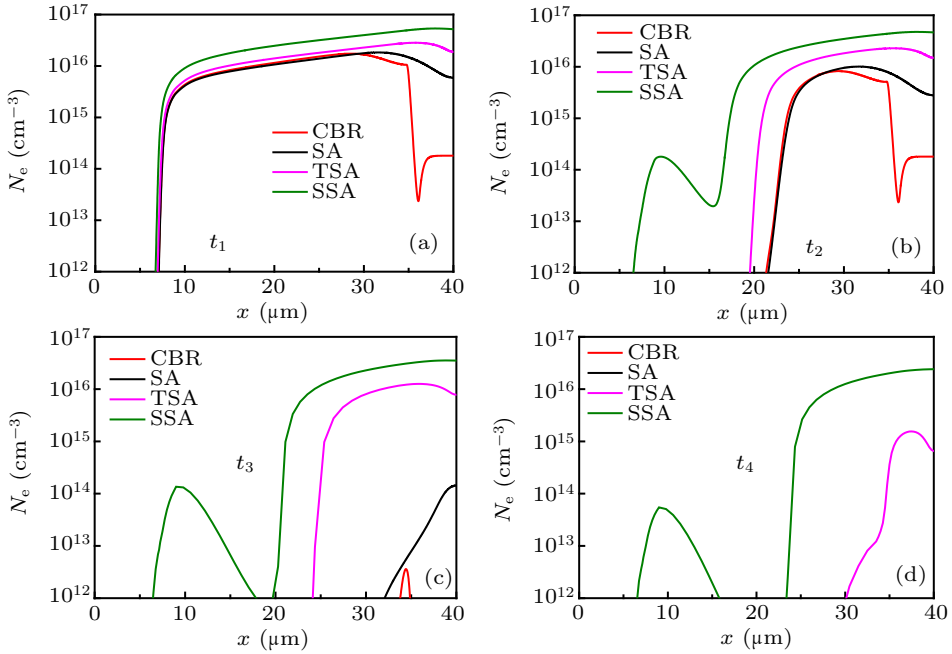


Fig. 6. Distributions of electron concentration N_e along x direction ($y = 4$ μm) of different LIGBTs at (a) t_1 period, (b) t_2 period, (c) t_3 period, and (d) t_4 period. (Curves at period t_1–t_4 are shown in Fig. 5).

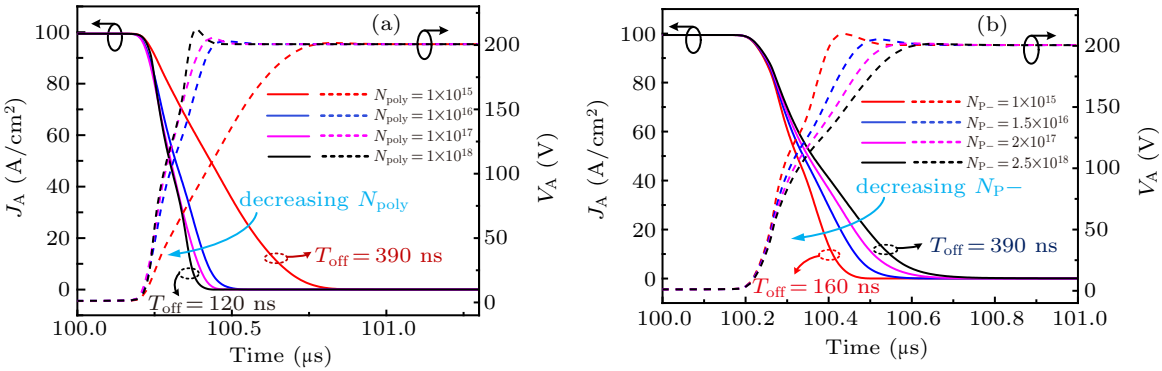


Fig. 7. Turn-off characteristics of CBR LIGBT (a) at different values of N_{poly} and (b) different values of N_{P-}.

Figure 7(a) shows the turn-off characteristics of CBR LIGBT at different values of N_{poly}. The CBR LIGBT has a T_{off} of 390 ns at an N_{poly} of 1×10^{15} cm^{-3}. The T_{off} decreases gradually with N_{poly} increasing due to R_1 decreasing, thus the turn-off loss E_{off} can be further reduced. Figure 7(b) shows the turn-off characteristics of CBR LIGBT at different values of N_{P-}. The T_{off} decreases from 390 ns to 160 ns with N_{P-} decreasing form 2.5×10^{16} cm^{-3} to 1×10^{16} cm^{-3} due to the enhanced $V_{barrier}$. Furthermore, a reasonable N_{poly} or N_{P-} is important to obtain a better trade-off between V_{on} and E_{off}.

3.3. Trade-off characteristic

Figure 8 displays the influences of N_{poly} and L on ΔV_{SB} and E_{off}. For the device with N_{poly} of 1×10^{15} cm^{-3}, it shows that the snapback-free characteristic occurs with the increase of L. However, it also results in a large E_{off}. For the device with N_{poly} of 1×10^{16} cm^{-3} and 1×10^{17} cm^{-3}, the ΔV_{SB} increases with L increasing, and a higher N_{poly} will bring a larger ΔV_{SB}. On the other hand, the E_{off} decreases with the increase of L, and increasing N_{poly} is beneficial to obtaining a lower E_{off}. Because L can be regarded as the width of the cross section of electron path from P-float to polysilicon layer, increasing L leads to a narrower path for electrons, which is helpful in reducing the value of E_{off}.

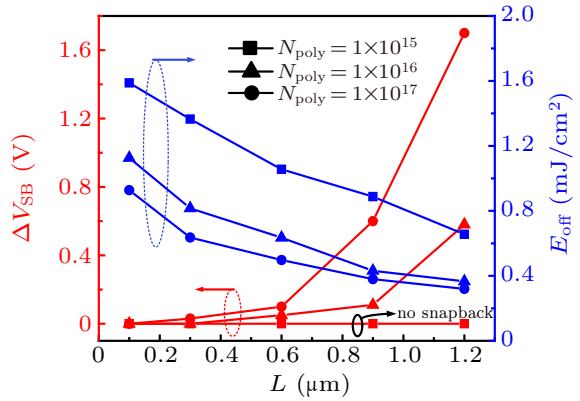


Fig. 8. Influences of N_{poly} and L on ΔV_{SB} and E_{off} of CBR LIGBT, with L shown in Fig. 1(b).

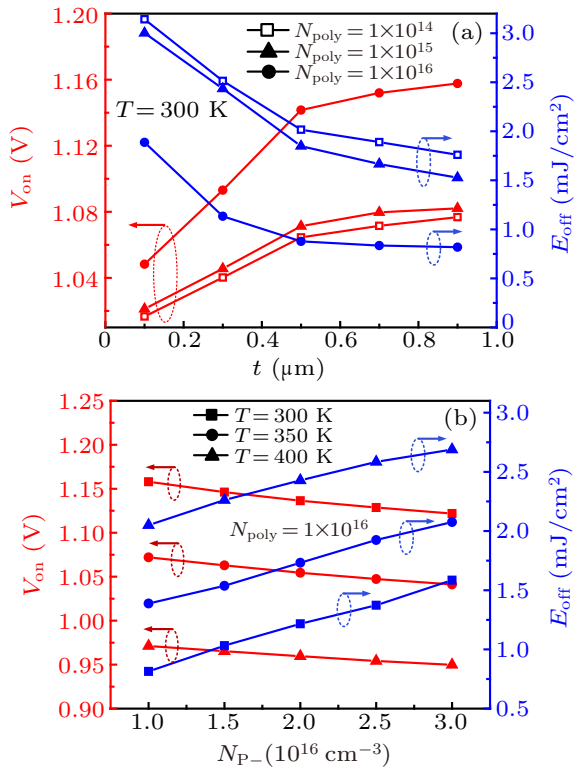


Fig. 9. Trade-off characteristics between V_{on} and E_{off}, showing (a) influences of N_{poly} and t on V_{on} and E_{off} of CBR LIGBT, and (b) the influences of temperature T and N_{P-} on V_{on} and E_{off} of CBR LIGBT, with t shown in Fig. 1(b).

Figure 9(a) displays the influences of N_{poly} and t on V_{on} and E_{off}. It is observed that increasing the width of the cross section t or N_{poly} will lead the value of V_{on} to increase. Simultaneously, the E_{off} decreases because the R_1 decreases with the increase of t and doping N_{poly}. Figure 9(b) shows the influences of temperature T and N_{P-} on V_{on} and E_{off}. The V_{on} decreases with T increasing due to a lower mobility, while the E_{off} increases. Meanwhile, the increasing N_{P-} can bring a higher E_{off} and a lower V_{on}.

Figure 10 shows the trade-off characteristics between V_{on} and E_{off} of different LIGBTs. The CBR LIGBT achieves the best trade-off characteristics in all LIGBTs. At the same V_{on} of 1.3 V, it realizes 85%, 73%, and 59.6% reductions in E_{off} compared with that of the SSA LIGBT, convention LIGBT, and TSA LIGBT, respectively. Additionally, at the same E_{off} of 1.5 mJ/cm^2, the V_{on} of the CBR LIGBT reduces by 26%, 24%, and 6% compared with that of the SSA LIGBT, conventional LIGBT and TSA LIGBT, respectively. Thus, the proposed device not only achieves the snapback-free characteristic, but also obtains a better trade-off characteristics between V_{on} and E_{off}.

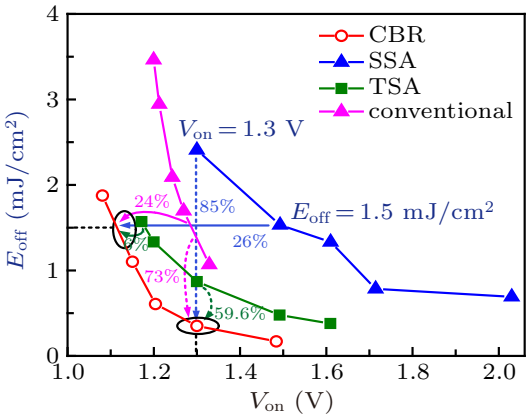


Fig. 10. Trade-off characteristics between V_{on} and E_{off} of different LIGBTs, with V_{on} values of different LIGBTs obtained at $J_A = 100$ A/cm^2 and E_{off} value calculated by varying concentration of P+ anode.

3.4. Key process of CBR LIGBT

Figure 11 shows the key process of fabricating the CBR LIGBTs. The main process can be divided into 8 steps. The oxide trench can be formed simultaneously with the SOI structure as shown in Fig. 11(a). In Figs. 11(b) and 11(c), the P-body, N-buffer, P+ anode, and N+ anode can be realized by using the multiple ion implantation. Then the oxide insulation layer and polysilicon are formed by deposition and etching process as shown in Figs. 11(d) and 11(e). Note that the secondary ion implantation is needed to reach the doping concentration of the polysilicon gate as shown in Fig. 11(f). Finally, the excess polysilicon and insulating layer are etched and electrodes are placed.

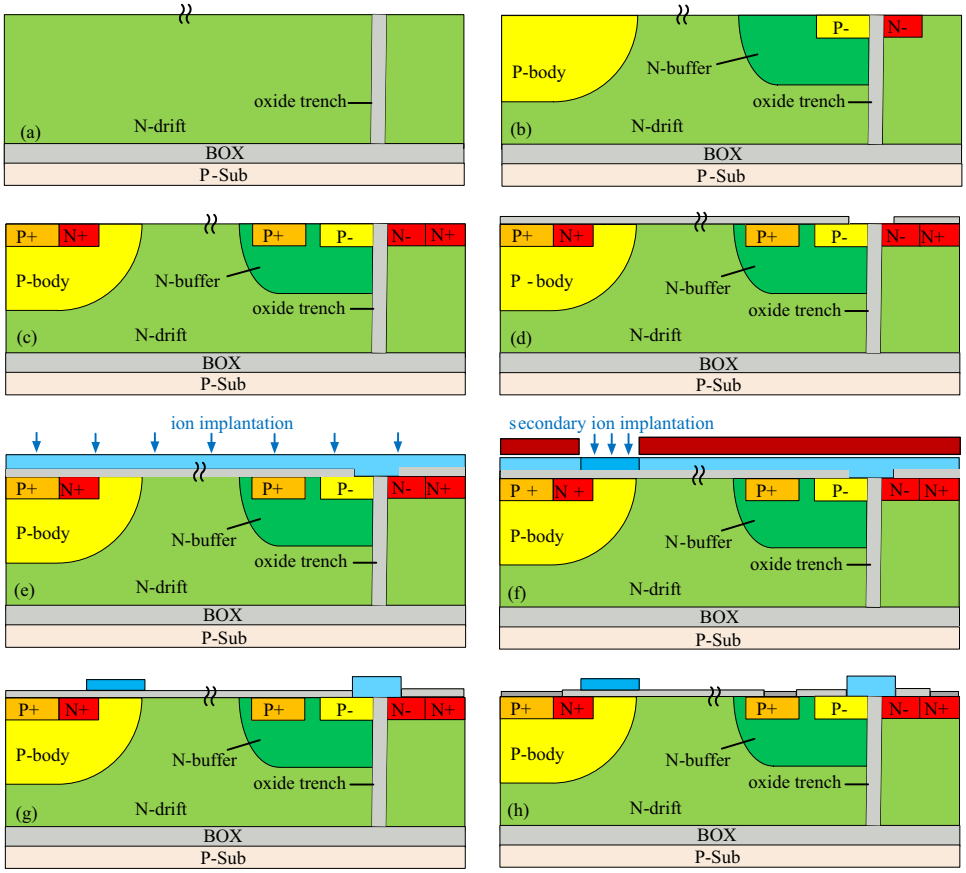


Fig. 11. Key process of fabricating CBR LIGBT, showing (a) oxide trench and SOI structure formation, (b) P-body, N-buffer, P-float, and N-float formations, (c) P+ and N+ cathode formations, P+ and N+ anode formations, (d) oxide layer formation by deposition and etching, (e) doping of the polysilicon layer, (f) secondary ion implantation to form polysilicon gate, (g) etching excess polysilicon, and (h) etching the oxide layer and place the electrode.

4. Conclusions

The controlled barrier and resistance CBR in the anode is introduced to control the V_{barrier} and R_{SA} for the SA LIGBT by adjusting the doping of the P-float, N-float and polisilicon layer. The results show that the CBR LIGBT not only achieves the snapback-free characteristic but also obtains better trade-off property between V_{on} and E_{off} than the SSA LIGBT, conventional LIGBT, and TSA LIGBT.

References

[1] Iwamuro N and Laska T 2017 *IEEE Trans. Electron Dev.* **64** 741
[2] Jiang H P, Zhang B, Chen W J, Li Z J, Liu C, Rao Z G and Dong B 2012 *IEEE Electron Dev. Lett.* **33** 417
[3] Yi B, Jia L, Zhang B K, Chen J J and Xiong Y 2020 *IEEE Trans. Electron Dev.* **67** 2058
[4] Deng G Q, Luo X R, Zhou K, He Q Y, Ruan X L, Liu Q, Sun T and Zhang B 2017 *Proc. ISPSD* 127
[5] Huang M M, Li J, Xie C J, Lai L and Gong M 2020 *Electron. Lett.* **56** 153
[6] Hu H, Kong M F, Yi B and Chen X B 2020 *IEEE Trans. Electron Dev.* **67** 1059
[7] Wu J Y, Huang H M, Yi B, Hu H, Hu H and Chen X B 2020 *IEEE J. Electron Dev. Soc.* **7** 1013
[8] Duan B X, Sun L C and Yang Y T 2019 *IEEE Electron Dev. Lett.* **40** 63
[9] Zhang B K, Kong M F, Yi B and Chen X B 2020 *IEEE Trans. Electron Dev.* **67** 2020
[10] Li J H, Tang Y, Zhang G J, Liu J, Liu K F, Hu B and Li W 2020 *IEEE Electron Dev. Lett.* **41** 573
[11] Zhang L, Zhu J, Sun W F, Chen M, Zhao M N, Huang X Q, Chen J J, Qian Y X and Shi L X 2017 *IEEE Trans. Electron Dev.* **64** 1187
[12] Chen W Z, Guo Q, He L J, Han Z S, Wang Y C and Li X Y 2017 *IEICE Electronics Express* **14** 1
[13] Pathirana V, Udugampola N, Trajkovic T and Udrea F. 2018 *IEEE Electron Dev. Lett.* **39** 866
[14] Chen W Z, Huang Y, He L J, Han Z S and Huang Y 2018 *Chin. Phys. B* **27** 088501
[15] Luo X R, Yang Y, Sun T, Wei J, Fan D, Ouyang D F, Deng G Q, Yang Y H, Zhang B and Li Z J 2019 *IEEE Trans. Electron Dev.* **66** 1390
[16] Tian T, Guo Y F, Yao J F, Zhang J, Wang K and Li M 2019 *IEEE J. Electron Dev. Soc.* **7** 725
[17] He Y T, Qiao M and Zhang B 2018 *Chin. Phys. B* **25** 127304
[18] Sin J K O and Mukherjee S 1991 *IEEE Electron Dev. Lett.* **12** 45
[19] Chul J H, Byeon D S, Oh J K, Han M K and Choi Y I 2000 *Proc. ISPSD* 149
[20] Park J M, Wagner S, Grasser T and Selberherr S 2003 *Solid-State Electronics* **48** 1007
[21] Zhang L, Zhu J, Sun W F, Du Y C, Yu H, Huang K Q and Shi L X 2015 *Proc. ISPSD* 49
[22] Zhu J, Zhang L, Sun W F, Chen M, Zhou F, Zhao M N, Shi L X, Gu Y and Zhang S 2016 *IEEE Trans. Electron Dev.* **63** 2003
[23] Chen W Z, Li S, Huang Y, Huang Y and Han Z S 2020 *IEEE J. Electron Dev. Soc.* In Press
[24] 'Taurus Medici DAVINCI User's Guides', Synopsys, Mountain View, CA, USA, 2014
[25] Zhou K, Sun T, Liu Q, Zhang B, Li Z J and Luo X R 2017 *Proc. ISPSD* 315